High-resolution measurements of excitations in superfluid ^{4}He beyond the roton

2001 J. Phys.: Condens. Matter 13 4421

(http://iopscience.iop.org/0953-8984/13/20/304)

INSTITUTE OF PHYSICS PUBLISHING JOURNAL OF PHYSICS: CONDENSED MATTER

J. Phys.: Condens. Matter **13** (2001) 4421–4434 www.iop.org/Journals/cm PII: S0953-8984(01)22997-X

High-resolution measurements of excitations in superfluid ^{4}He beyond the roton

J V Pearce[1,6], R T Azuah[1], B Fåk[2,3], A R Sakhel[4], H R Glyde[4] and W G Stirling[1,5]

[1] Department of Physics, Oliver Lodge Laboratory, University of Liverpool, Liverpool L69 7ZE, UK
[2] Commissariat à l'Energie Atomique, Département de Recherche Fondamentale sur la Matière Condensée, SPSMS/MDN, 38054 Grenoble Cédex 9, France
[3] ISIS Facility, Rutherford Appleton Laboratory, Chilton, Didcot OX11 0QX, UK
[4] Department of Physics and Astronomy, University of Delaware, Newark, DE 19716, USA
[5] ESRF, rue Jules Horowitz, BP 220, 38043 Grenoble Cédex 9, France

E-mail: jvpearce@liv.ac.uk

Received 16 March 2001

Abstract

High-resolution neutron inelastic scattering studies of the wavevector and temperature dependence of the excitation spectrum of ^{4}He in the superfluid and normal-fluid phases have been made in the wavevector region 'beyond the roton', $2.0 < Q < 3.6$ Å^{-1}, at a pressure of 20 bar. The scattering in this region exhibits two separate components: a sharp peak at low energies and a broader continuum at higher energies. The relative intensity of these two peaks is Q-dependent. We find that the two-roton energy, 2Δ, is never exceeded by the sharp peak at this pressure. The data are compared with the density–quasiparticle model of Glyde and Griffin and a tentative analysis of the temperature dependence of the condensate fraction n_0 is made.

1. Introduction

In the superfluid phase of liquid ^{4}He, where there are a finite number of atoms in the Bose condensate, the excitation spectrum is dominated by the sharp phonon–maxon–roton curve for wavevectors $Q < 2$ Å^{-1}. The excitations beyond the roton ($Q > 2$ Å^{-1}) are not well determined experimentally nor understood at a microscopic level, partly because very high instrumental resolution is required to resolve the different components of the observed scattering [1]. However, the introduction by Glyde and Griffin (G–G) of the density–quasiparticle interpretation [2, 3] has motivated several recent studies of the behaviour and temperature dependence of the excitation spectrum in this region [4–7].

[6] Author to whom any correspondence should be addressed.

0953-8984/01/204421+14$30.00

In this paper all energies $\hbar\omega$ are represented by ω to be consistent with related theoretical papers. One issue still outstanding is the upper limit of the excitation energy of the single-excitation component ω_Q observed in the dynamic structure factor $S(Q, \omega)$. Pitaevskii [8] postulated that ω_Q should never exceed 2Δ, where Δ is the roton excitation energy. The dispersion is expected to flatten out at 2Δ with increasing Q. This is because when $\omega_Q > 2\Delta$ the single excitation has sufficient energy to decay into two rotons and should cease to exist as a well-defined excitation. In early neutron scattering measurements, Cowley and Woods [9] and Smith *et al* [10] found that ω_Q *exceeded* 2Δ and that a single-excitation peak still remained. Recent high-resolution studies [1] seem to indicate that $\omega_Q < 2\Delta$ at SVP.

In this work, we have measured $S(Q, \omega)$ for liquid helium beyond the roton at a pressure of 20 bar in order to determine whether $\omega_Q < 2\Delta$ is a general feature of the excitation spectrum or a particularity at saturated vapour pressure. The experimental aspects are discussed in section 2. Section 3 outlines the Glyde–Griffin interpretation and a specific parametrization thereof which will be used for analysing our data. The results of the measurements are presented and analysed in section 4 using both a phenomenological approach and the G–G interpretation. Section 5 concludes the paper.

2. Experimental details

Neutron inelastic scattering measurements were performed on the IRIS inverted-geometry time-of-flight spectrometer at the ISIS pulsed neutron source. A final neutron energy of $E_f = 7.3867$ meV (wavevector 1.8882 Å^{-1}) was selected by using the (004) Bragg reflection of an array of pyrolytic graphite (PG) analysers cooled to 25 K to reduce background from thermal diffuse scattering [11]. The energy resolution at the elastic position is approximately 50 μeV in this configuration, although the energy resolution is Q-dependent as we will discuss below. There are 51 detector elements, each with an associated $S(\phi, \omega)$, where ϕ is the scattering angle and ω is the frequency.

Approximately 148 cm^3 of high-purity ^{4}He was condensed into a cylindrical aluminium sample cell (internal diameter 56 mm, internal height 61 mm). Inside the cell were placed three 0.5 mm thick horizontal disc-shaped cadmium spacers (diameter 56 mm) regularly spaced vertically to minimize multiple-scattering events. Between these discs were placed three vertically positioned aluminium foil cylinders (diameter 45 mm, height 20 mm, thickness 0.125 mm). The sample was pressurized to 20 bar and cooled in a ^{3}He sorption cryostat.

Measurements were made at temperatures of 0.60, 1.29, 1.70 and 2.10 K. Temperature regulation was stable to within ± 0.01 K. The superfluid transition temperature of liquid ^{4}He at a pressure of 20 bar is $T_\lambda = 1.928$ K. The constant, flat empty-cell background scattering was measured at 4.5 K and subtracted from the helium scattering.

2.1. Data reduction

IRIS records data at constant scattering angles ϕ. For comparison with other measurements and theoretical descriptions, it is expedient to express the data in constant-Q form. For this reason an algorithm was developed to take data taken along lines of constant ϕ in the (Q, ω) plane and rebin onto a rectangular (Q, ω) grid. We assume that the detectors are sufficiently close together that the finite-width strip in (Q, ω) described by each detector is adjacent to the neighbouring strips. The width of the constant-Q bins (0.05 Å^{-1}) was chosen to be considerably larger than the Q-width of the detectors. Figure 1 shows the range of (Q, ω) space available to IRIS.

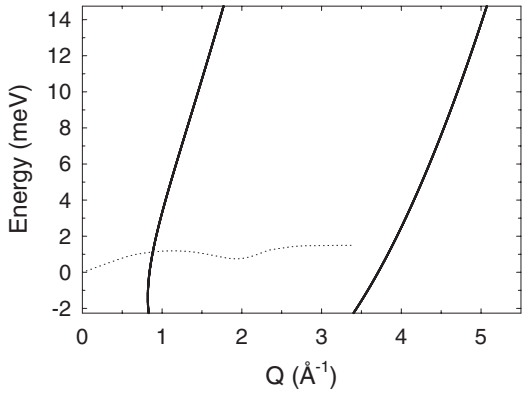

Figure 1. Constant-ϕ loci in (Q, ω) space representing the first and last detectors of IRIS using the PG(004) analyser configuration. The dispersion curve of superfluid ^{4}He at SVP is also shown (dotted line).

2.2. Instrumental resolution

2.2.1. Geometrical calculation. In any neutron scattering experiment requiring extraction of linewidths, some measure of the instrumental resolution broadening is needed. This is simple at and around the roton wavevector ($Q < 2$ Å^{-1}), where the observed broadening can be attributed solely to instrumental resolution broadening, but this is not necessarily true in other regions of the dispersion curve. Resolution issues are particularly important at wavevectors higher than the roton, where the excitation peak position, ω_Q, and its weight, Z_Q, are changing rapidly with Q. In these regions we expect considerable broadening in Q and ω. By approximating the resolution function of IRIS by Gaussians in both ω (FWHM $\Delta\omega$) and Q (FWHM ΔQ), Crevecoeur *et al* [12] have formulated an overall quantity, $\Delta R(Q)$, which represents the FWHM of the overall resolution function:

$$\Delta R(Q) = \sqrt{(\Delta\omega)^2 + (\Delta Q)^2\left(\frac{\mathrm{d}\omega_Q}{\mathrm{d}Q}\right)^2} \tag{1}$$

where $\mathrm{d}\omega_Q/\mathrm{d}Q$ is given by the gradient of the ^{4}He dispersion curve at that point. The data in (Q, ω) can then be convoluted with this Gaussian to enable extraction of the intrinsic excitation linewidth. Thus (1) allows the determination of the resolution function of IRIS at any position in (Q, ω) space for this measurement.

2.2.2. Summation over Gaussians. The method outlined above gives the expected broadening when $\mathrm{d}\omega/\mathrm{d}Q$ and $\mathrm{d}Z/\mathrm{d}Q$ are high, but it does not give any indication of the effect on the lineshape. It is important to gain some idea of the qualitative lineshape arising from such broadening. The simplest means of doing this is to sum the response over a given range of Q. The observed scattering intensity $I(Q, \omega)$ is a convolution of the dynamic structure factor $S(Q, \omega)$ and the resolution function $R(Q, \omega)$. $S(Q, \omega)$ can be approximated by a δ-function at $\omega_{Q'}$ with weight $Z_{Q'}$. After integrating out the energy variable in the resolution convolution, we obtain

$$I(Q, \omega) = \int_{-\infty}^{\infty} Z_{Q'} R(Q - Q', \omega - \omega_{Q'})\, \mathrm{d}Q'. \tag{2}$$

However, as the Q-resolution of IRIS is dominated by the detector size, we can reasonably approximate it to be rectangular, of width ΔQ. By assuming that the energy resolution takes

the form of a Gaussian, equation (2) can then be written as

$$I(Q,\omega) = \int_{Q-\Delta Q/2}^{Q+\Delta Q/2} Z_{Q'} R_0 \exp\left(-\frac{(\omega-\omega_{Q'})^2}{2\sigma_\omega^2}\right) \mathrm{d}Q' \tag{3}$$

over a finite Q-range ΔQ. R_0 is chosen such that

$$\int_{-\infty}^{\infty} R(Q,\omega)\,\mathrm{d}Q\,\mathrm{d}\omega = 1.$$

The quantities $\omega_{Q'}$ and $Z_{Q'}$ were expanded to first order in Q:

$$\omega_{Q'} = \omega_Q + \frac{\mathrm{d}\omega_Q}{\mathrm{d}Q}(Q'-Q) \qquad Z_{Q'} = Z_Q + \frac{\mathrm{d}Z_Q}{\mathrm{d}Q}(Q'-Q).$$

The expression in (3) was evaluated numerically for $Q = 2.5$ Å^{-1}, with Q-bin widths ΔQ chosen over a wide range to determine the effect of different ΔQ on the observed broadening. The value of σ was taken from the HWHM of the single-excitation peak at this wavevector at low temperature ($\sigma_{Q=2.5} = \Gamma/(2\ln 2)^{1/2} = 0.093$ meV). The results of the calculation are presented in figure 2, which demonstrates the symmetrical broadening exhibited by the model, the width of which increases as the Q-binning is widened. Of primary interest is the fact that we observe no significant *asymmetrical* broadening of the energy resolution function for small Q-bin widths ΔQ (i.e. $\Delta Q < 0.2$ Å^{-1}). It is therefore reasonable to model the instrumental resolution using a symmetrical function with a width given by (1).

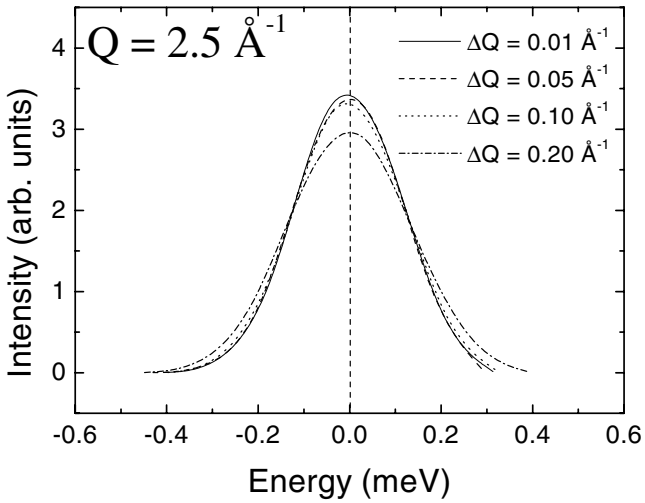

Figure 2. Calculated resolution broadening in ω resulting from binning in a finite-Q element of width ΔQ centred at $Q = 2.5$ Å^{-1}. This represents the maximum broadening possible because at this wavevector the energy and intensity of the response are changing most rapidly with Q. The calculated response is normalized to unity.

3. Theory

3.1. The Glyde–Griffin approach

The density–quasiparticle interpretation of G–G [2, 3] provides a microscopic interpretation of the behaviour of liquid ^{4}He above and below T_λ. This scheme qualitatively explains the

temperature dependence of the phonon–roton excitation by specifically including the Bose condensate, and allows semi-quantitative comparison with neutron scattering measurements. In the normal fluid at low Q, the broadened phonon is interpreted by G–G as a zero-sound mode, i.e. a collective density fluctuation. As Q increases, this mode becomes heavily damped and the remaining broad contribution is due to weakly interacting particle–hole excitations. In the superfluid, the single-quasiparticle excitation is 'coupled' into the density-fluctuation spectrum by the Bose condensate. The density and the single-quasiparticle excitations become one and the same mode, so there are no independent quasiparticle excitations at lower energy to which the common mode can decay. This strong coupling with the condensate gives rise to the well-defined continuous phonon–roton dispersion curve.

3.2. Formulation of the model

The quantity measured in a neutron scattering experiment is the dynamic structure factor $S(Q, \omega)$. This is proportional to the imaginary part of the total dynamic susceptibility $\chi(Q, \omega)$ as described in the dielectric formulation [2, 3]:

$$S(Q, \omega) \propto \Im(\chi(Q, \omega)) \tag{4}$$

where

$$\chi = \frac{\bar{\chi}}{\epsilon} \tag{5}$$

where ϵ is the dielectric function. The barred quantities refer to the irreducible contribution as expressed in the dielectric formalism. The key aspect of the density–quasiparticle interpretation is the separation of the atoms in the Bose condensate from those above. This is achieved by the decomposition of $\bar{\chi}$ into two parts:

$$\bar{\chi} = \bar{\chi}_R + \bar{\chi}_S. \tag{6}$$

The first part in (6), $\bar{\chi}_R$, describes the regular density excitations, involving only states above the condensate. It can be separated into a single-quasiparticle–hole component and a multiparticle component:

$$\bar{\chi}_R = \bar{\chi}_o + \bar{\chi}_m \tag{7}$$

The multiparticle component $\bar{\chi}_m$ is neglected in the Glyde–Griffin model. Note that while this may be an acceptable approximation around the phonon–maxon–roton wavevectors, it may cause significant problems when modelling the response at wavevectors beyond the roton, as the multiparticle continuum forms an increasingly significant contribution to the observed scattering spectrum as Q increases.

The second part in (6), $\bar{\chi}_S$, represents coupling with the condensate:

$$\bar{\chi}_S = \bar{\Lambda}\bar{G}\bar{\Lambda}. \tag{8}$$

$\bar{G}$ is the uncoupled single-particle Green's function which describes the propagation of a single-quasiparticle excitation and is coupled into the density spectrum χ by the condensate. The coupling of $\bar{G}$ into the density spectrum is described by the Bose vertex function $\bar{\Lambda}$, which disappears above T_λ:

$$\bar{\Lambda}(Q, \omega) = \sqrt{n_0(T)}(1 + P(Q, \omega)) \tag{9}$$

where $P(Q, \omega)$ is a complicated function related to the terms describing the interference between one- and two-particle excitations. Equation (9) contains the temperature dependence of this model. This arises from $n_0(T)$, described by the ideal-Bose-gas result:

$$n_0(T) = n_0(0)[1 - (T/T_\lambda)^\gamma]. \tag{10}$$

For an ideal gas, $\gamma = 1.5$. For liquid ^{4}He, which is a strongly interacting Bose system, γ has been estimated to be 4.7 ± 1.2 [13].

At higher wavevectors, beyond the roton, interactions within the liquid are relatively weak and the model $S(Q, \omega)$ is expected to be composed of three weakly related components:

- A sharp, single-quasiparticle peak scaling with temperature to disappear at T_λ, which arises from $\bar{G}$ and the first term in $\bar{\Lambda}$.
- A broader, two-quasiparticle component scaling with temperature in a manner similar to that of the single-quasiparticle peak. It arises from the second term in $\bar{\Lambda}$ centred at approximately twice the single-excitation energy.
- A broad, temperature-independent regular density peak which arises from $\bar{\chi}_R$.

3.3. Application to experimental data

Above T_λ only density excitations are present and the dynamic structure factor is given by the uncoupled density response [3]:

$$S(Q,\omega) = \frac{F(Q)}{\pi}[n_B(\omega)+1]\frac{4\omega\bar{\omega}_0\Gamma_0}{(\omega^2-\bar{\omega}_0^2)^2+(2\omega\Gamma_0)^2} \tag{11}$$

where $F(Q)$ is the Q-dependent weight, $\bar{\omega}_0$ is the energy of the regular density peak and Γ_0 is the corresponding HWHM. The Bose occupation factor is $n_B(\omega) = (\mathrm{e}^{\omega/k_BT}-1)^{-1}$. At temperatures below T_λ,

$$S(Q,\omega) = \frac{F(Q)}{\pi}[n_B(\omega)+1]\frac{(4\omega\bar{\omega}_0\Gamma_0)(\omega^2-\bar{\omega}_{SP}^2)^2}{\left[(\omega^2-\omega_0^2)(\omega^2-\omega_{SP}^2)\right]^2+\left[2\omega\Gamma_0(\omega^2-\bar{\omega}_{SP}^2-\Delta_{SP})\right]^2} \tag{12}$$

where

$$(\omega^2-\omega_0^2)(\omega^2-\omega_{SP}^2) \equiv (\omega^2-\bar{\omega}_0^2)(\omega^2-\tilde{\omega}_{SP}^2)-\Delta_{SP}\alpha_0. \tag{13}$$

Here $\tilde{\omega}_{SP}^2 = \bar{\omega}_{SP}^2+\Delta_{SP}$ and $\tilde{\omega}_0^2 = \bar{\omega}_0^2+\alpha_0$. $\bar{\omega}_{SP}$ and $\bar{\omega}_0$ are interpreted as being the uncoupled quasiparticle and density-fluctuation energies (poles), respectively, in the superfluid. ω_{SP} and ω_0 are the shifted energies due to coupling via the condensate. $S(Q, \omega)$ can be described by five parameters: $\bar{\omega}_0$, the regular density response energy; Γ_0, its width; $\bar{\omega}_{SP}$, the single-particle mode energy; and Δ_{SP} and α_0, which are coupling parameters. All parameters are held independent of temperature except Δ_{SP} which represents the coupling between the quasiparticle and regular density response via the condensate. The temperature dependence of $S(Q, \omega)$ in (12) therefore follows from $\Delta_{SP}(T) \propto n_0(T)$. Explicitly,

$$\Delta_{SP}(T) = \Delta_{SP}(0)[1-(T/T_\lambda)^\gamma]. \tag{14}$$

Thus the experimental determination of the temperature dependence of Δ_{SP} should provide a direct measure of the condensate fraction n_0.

4. Analysis

4.1. Results

The roton energy Δ was determined at $T = 0.6$ K by making a parabolic fit to the sharp excitation peak positions around the roton minimum ($Q \sim 2$ Å^{-1}) as described elsewhere [14]. At this temperature, $\Delta = 0.652(1) \pm 0.001(4)$ meV ($2\Delta = 1.304(2)$ meV), the roton wavevector $Q_R = 2.04 \pm 0.01$ Å^{-1} and the roton effective mass $\mu_R = 0.224 \pm 0.029\, m_{^4\mathrm{He}}$.

Figure 3 is a colour map of the excitation spectra in (Q, ω) space in the superfluid and normal-fluid phases. The top panel demonstrates the splitting of the dispersion into two

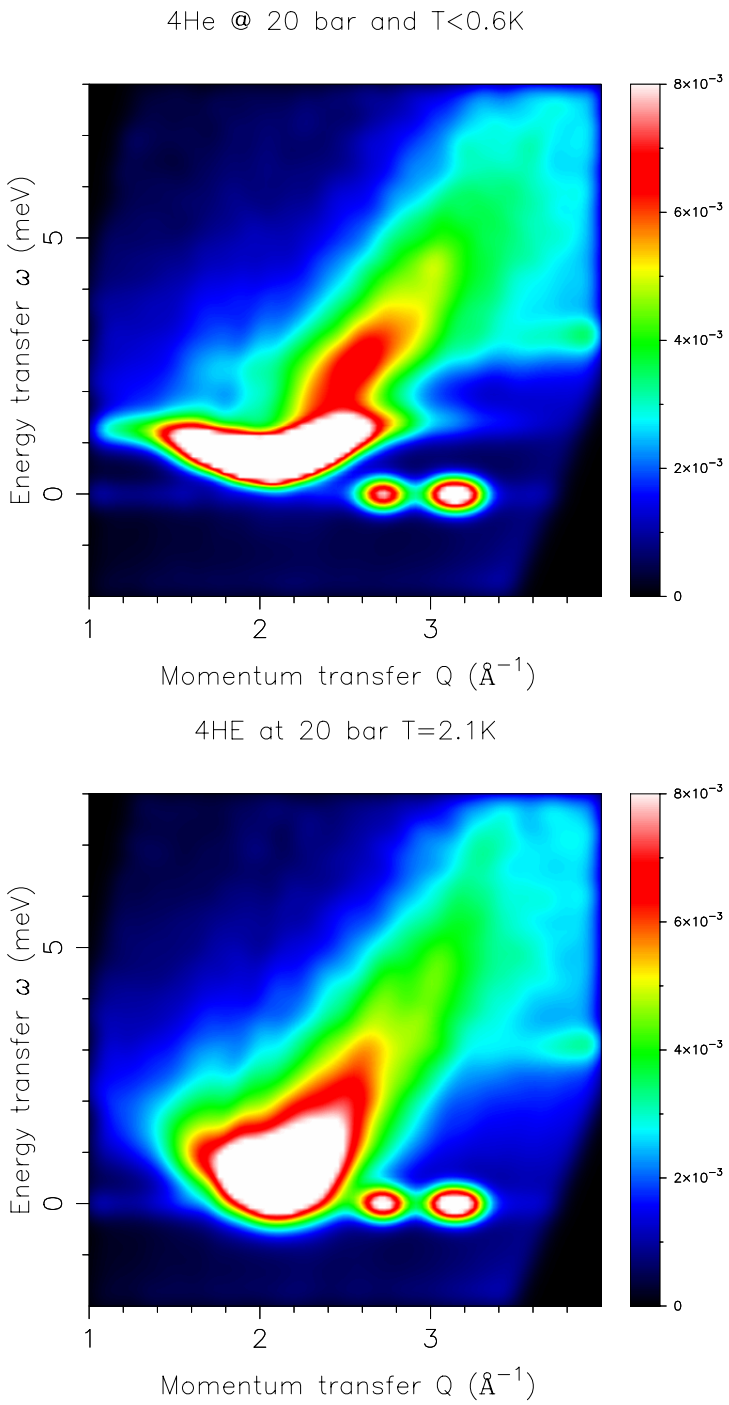

Figure 3. Colour plots showing the observed $S(Q, \omega)$ for liquid ^{4}He at 20 bar at temperatures of 0.6 K (top panel) and 2.1 K (bottom panel). The full intensity of the sharp single-excitation peak has been truncated to display the rich multiphonon structure (higher energy). The two isolated pockets of scattering on the elastic line ($Q \sim 3$ Å^{-1}) are due to Bragg scattering from the Al sample cell.

branches at around 2.5 Å^{-1}: a rapidly disappearing sharp peak which continues at an energy of 2Δ and a diverging broad peak which extends to higher energies. These two branches represent the two main components of the scattering spectrum in the models described in later sections. The bottom panel shows the substantial broadening of the response at higher temperature. A series of cuts at constant Q are presented in figure 4. At around $Q = 2.3$ Å^{-1} we observe a transfer of weight from the sharp, low-energy phonon–roton mode to the broad, high-energy multiparticle continuum, which steadily continues as Q increases. The dispersion flattens at around 3 Å^{-1}. The dispersion disappears completely for $Q > 4$ Å^{-1}, where the Doppler-broadened recoil scattering becomes the most prominent feature in the excitation spectrum.

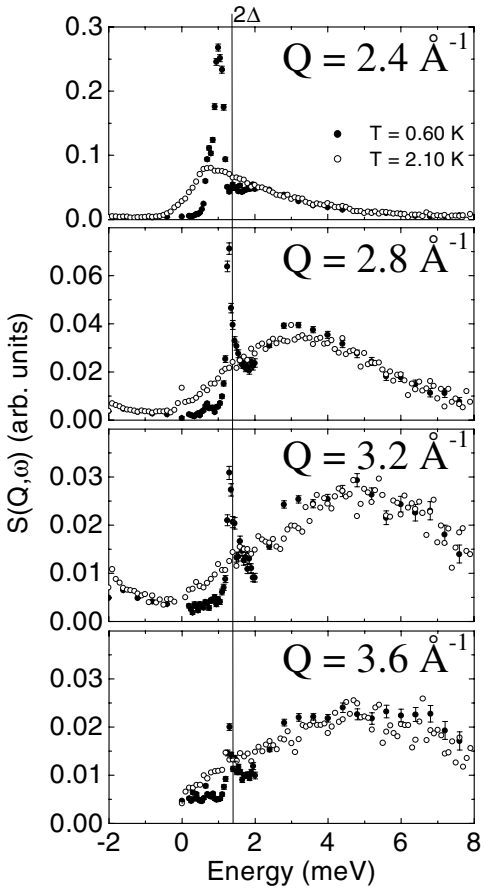

Figure 4. $S(Q, \omega)$ for liquid ^{4}He at 20 bar at representative wavevectors. The transfer of intensity from the sharp single-excitation peak to the broad multiphonon continuum can be seen with increasing Q (top to bottom). Note that 2Δ is not exceeded at any wavevector.

The temperature dependence of $S(Q, \omega)$ is considered explicitly in section 4.3 where figures 7 and 8 show the variation with T at $Q = 3.0$ Å^{-1}. The weight of the single-excitation peak is seen to be strongly temperature dependent. As the temperature increases, it becomes weaker relative to the broad component, until above T_λ it disappears altogether. This is what would be expected if the excitation is linked to the condensate. The higher-energy region is seen to remain roughly independent of temperature.

4.2. Damped harmonic oscillator (DHO) model plus ad hoc Gaussian components

Quantitative analysis of the data was performed with the aim of extracting the energy, linewidth and peak strength of the single-excitation peak. The sharp single-excitation peak was modelled using the single-DHO expression:

$$S(Q,\omega) = \frac{Z_Q}{\pi}[n_B(\omega)+1]\left[\frac{\Gamma_Q}{(\omega-\omega_Q)^2+\Gamma_Q^2} - \frac{\Gamma_Q}{(\omega+\omega_Q)^2+\Gamma_Q^2}\right] \tag{15}$$

where Z_Q is the single-excitation weight, Γ_Q is the HWHM and ω_Q is the excitation energy. To give a good description of the response, it is necessary to convolute (15) with the resolution function. The experimentally observed low-energy single-excitation peak has an asymmetric broadening on the high-energy side, originating from its hybridization with the multiparticle continuum. To describe this asymmetry, we used a DHO function to model the single excitation, and a less intense Gaussian component centred at a slightly higher energy than the single-excitation energy. Two additional *ad hoc* Gaussians were used to model the high-energy broad component of the scattering. An example of the quality of data fitting is shown in figure 5. This approach has little physical justification; it should be thought of only as a convenient way of describing the single-excitation peak.

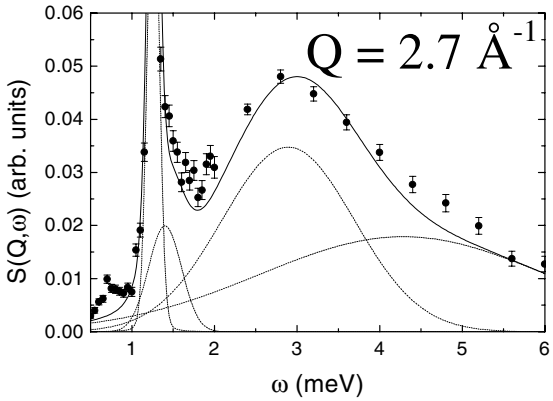

Figure 5. $S(Q,\omega)$ for liquid ^{4}He at $Q = 2.7$ Å^{-1}, 20 bar and $T = 0.6$ K illustrating the quality of fitting using the DHO model + *ad hoc* Gaussian components.

Fits to the data at 0.6 K for $2.0 < Q < 3.6$ Å^{-1} yield the position of the single-excitation peak, listed in table 1. Figure 6 shows the dispersion curve at this temperature derived using the above technique. We find that the single-excitation energy ω_Q does not exceed the two-roton energy 2Δ.

4.3. Glyde–Griffin parametrization

We report on two different methods of implementing the G–G fitting technique. In the first, the G–G model is parametrized from the high-temperature data above T_λ and the relevant parameters are kept fixed during fitting to superfluid data. In the second, the model is parametrized from the normal-fluid data as before, but no attempt is made to keep the relevant parameters fixed thereafter.

4.3.1. Fixed (high-T) parameters. To examine the temperature dependence of the data and to gain some indication of the behaviour of Δ_{SP}, the data at 3.0 Å^{-1} were selected for detailed

Table 1. The energy ω_Q and weight Z_Q of the sharp peak in $S(Q,\omega)$ of liquid ^{4}He at 20 bar and $T = 0.6$ K at Q-values beyond the roton, obtained using *ad hoc* fitting components. $2\Delta = 1.304(2) \pm 0.004$ meV.

Q (Å^{-1})	ω_Q (meV)	Z_Q (arbitrary units)
2.0	0.652 ± 0.002	0.138 ± 0.007
2.2	0.707 ± 0.004	0.160 ± 0.005
2.4	0.979 ± 0.003	0.100 ± 0.002
2.6	1.203 ± 0.002	0.037 ± 0.001
2.8	1.287 ± 0.002	0.013 ± 0.001
3.0	1.305 ± 0.003	0.006 ± 0.002
3.2	1.313 ± 0.003	0.005 ± 0.001
3.4	1.294 ± 0.005	0.003 ± 0.001
3.6	1.295 ± 0.004	0.003 ± 0.001

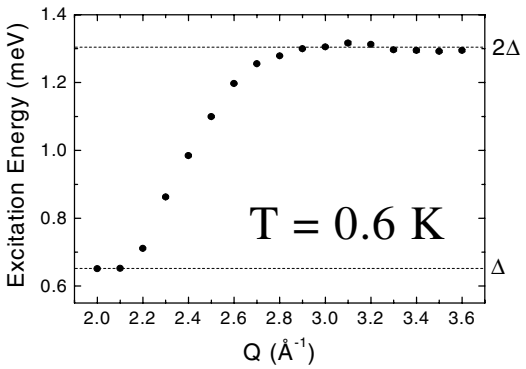

Figure 6. Energy dispersion of ^{4}He at $T = 0.6$ K determined using *ad hoc* fitting components described in the text. The error bars are smaller than the data points. Here we see that 2Δ is not exceeded.

study, since the dispersion curve is approximately flat and broadening of the response due to finite Q-binning can be ignored.

First, the data are considered at $T = 2.1$ K, which is above T_λ and where there is no observed single-excitation peak. The response can be described by (11). Least-squares fitting of (11) yields the parameters $F(Q)$, Γ_0 and $\bar{\omega}_0$.

Second, the data are considered at the three temperatures 0.6, 1.29 and 1.7 K. These temperatures are below T_λ and the response can be described by (12). The quantities $F(Q)$, Γ_0 and $\bar{\omega}_0$ are kept fixed at the values obtained at $T = 2.1$ K. The remaining parameters in the fit are $\bar{\omega}_{SP}$, Δ_{SP} and α_0. Since $\bar{\omega}_{SP}$ is given by the position of the 'dip' in intensity between the two major components of the scattering, its value can be fixed at this observed position of $\bar{\omega}_{SP} = 1.3$ meV. We now have two remaining parameters to be fitted: Δ_{SP} and α_0. These two parameters are allowed to vary freely during the fitting procedure. Results of the fits are shown in figure 7. The fitted G–G parameters are presented in table 2.

4.3.2. Free (high-T) parameters. As before, the data are considered at $T = 2.1$ K, which is above T_λ and where there is no observed single-excitation peak. Least-squares fitting of (11) yields the parameters $F(Q)$, Γ_0 and $\bar{\omega}_0$.

Again, the data are considered at the three temperatures, 0.6, 1.29 and 1.7 K. These temperatures are below T_λ and the response can be described by (12). However, equation (12)

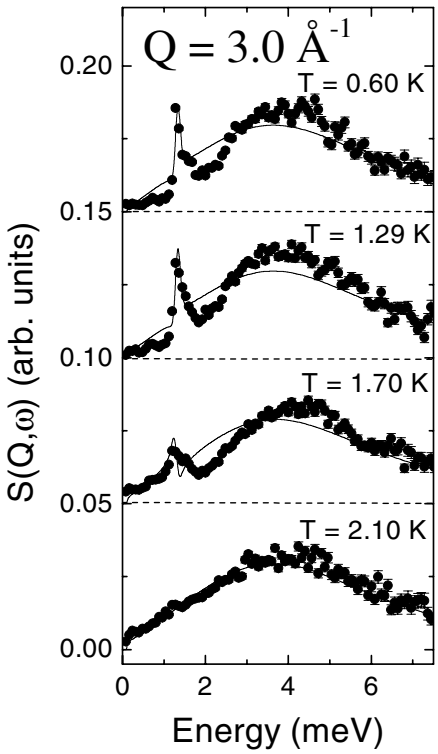

Figure 7. The temperature dependence of the $S(Q, \omega)$ observed on IRIS at $Q = 3.0$ Å^{-1}. The resolution-broadened G–G fit to the data is shown, with $F(Q)$, Γ_0 and ω_0 parametrized from the data above T_λ.

Table 2. The temperature dependence of the best-fit parameters of the Glyde–Griffin model for $Q = 3.0$ Å^{-1} at 20 bar. In the upper half of the table, $F(Q)$, Γ_0 and ω_0 were fixed to the $T = 2.1$ K values, while they were free to vary in the lower half.

T (K)	$F(Q)$ (arbitrary)	Γ_0 (meV)	$\bar{\omega}_0$ (meV)	ω_{SP} (meV^2)	Δ_{SP} (meV^2)	α_0 (meV^2)
0.60	(0.280)	(3.45)	(4.82)	1.30	0.0492	10.5
1.29	(0.280)	(3.45)	(4.82)	1.30	0.0498	10.4
1.70	(0.280)	(3.45)	(4.82)	1.30	−0.160	15.8
2.10	0.280	3.45	4.82	—	—	—
0.60	0.200	2.00	4.50	1.30	0.0500	7.58
1.29	0.220	2.00	4.40	1.30	0.0500	7.54
1.70	0.210	2.10	4.70	1.30	0.0262	0.997
2.10	0.280	3.45	4.82	—	—	—

provides a better description of the data if the quantities $F(Q)$, Γ_0 and $\bar{\omega}_0$ are allowed to vary freely around the high-temperature values. Δ_{SP} and α_0 are then established in the same manner as described above. Results of the fits are shown in figure 8. The fitted G–G parameters are presented in tables 2 and 3. It is evident that allowing the 'broad-component' parameters to vary from their high-temperature values enables a closer match between the G–G model and the experimental data to be achieved.

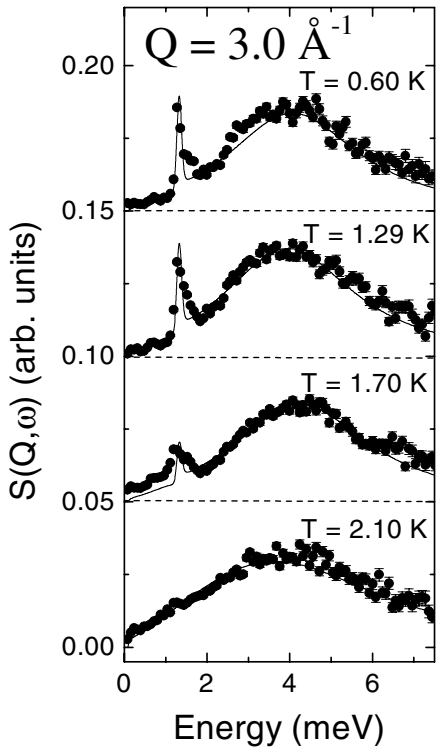

Figure 8. As figure 7, but with $F(Q)$, Γ_0 and ω_0 allowed to vary in the fitting procedure.

Moreover, having extracted the values of Δ_{SP} from the parametrization it is possible to see whether Δ_{SP} provides a measure of the condensate fraction n_0 as described by (14). The most recent value of n_0 determined by high-momentum-transfer neutron scattering measurements is $n_0 = 7.25 \pm 0.75\%$ [15]. To make the comparison, we assume that $\Delta_{SP}(0) \sim \Delta_{SP}(0.6) \equiv n_0 = 7.25\%$. The experimentally determined values of $\Delta_{SP}(T)$ can then be compared with the expected values provided by (14). Such a comparison is shown in figure 9. Firm conclusions about the relationship between Δ_{SP} and n_0 would require data at a larger number of temperatures. However, we note that the scaling of Δ_{SP} as depicted in figure 9 is not inconsistent with the assertion that $\Delta_{SP} \propto n_0$.

Table 3. The Q-dependence of the best-fit parameters of the Glyde–Griffin model for $T = 1.29$ K at 20 bar.

Q (Å^{-1})	Z_Q (arbitrary)	Γ_0 (meV)	$\bar{\omega}_0$ (meV)	ω_{SP} (meV)	Δ_{SP} (meV^2)	α_0 (meV^2)
2.6	1.73	1.92	3.38	1.12	0.104	2.97
2.8	1.74	1.96	3.86	1.18	0.269	6.42
3.0	2.04	2.13	4.54	1.21	0.219	9.96
3.2	2.77	3.02	5.45	1.23	0.090	5.52
3.4	3.60	4.40	6.30	1.23	0.103	15.4
3.6	3.28	4.40	5.96	1.23	0.053	14.2

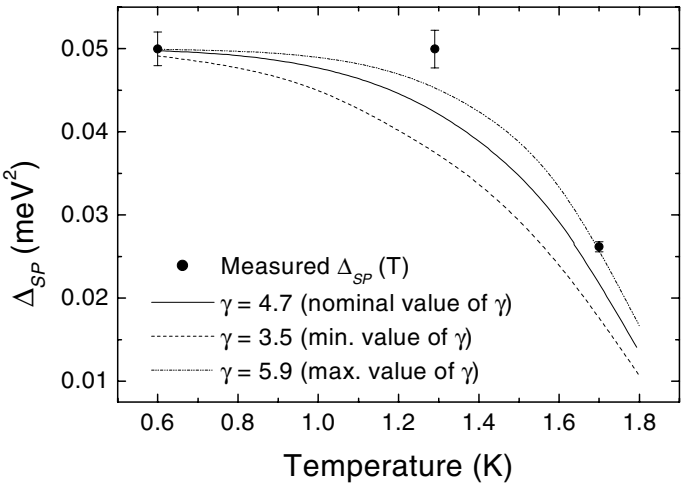

Figure 9. The temperature dependence of Δ_{SP} (data points). The solid line represents the expected temperature dependence if Δ_{SP} scales with the condensate fraction, i.e. $\Delta_{SP}(T) \propto n_0(T)$.

5. Conclusions

Neutron inelastic scattering measurements have been performed on superfluid ^{4}He at 20 bar for four temperatures above and below T_λ over a wide range of energies and wavevectors in the region beyond the roton. The high resolution and good statistical precision of the data enable clear separation of the two major features of $S(Q, \omega)$ in this region; a sharp, temperature-dependent low-energy peak 'sitting' on a broad, largely temperature-independent higher-energy peak. A transfer of weight between the two peaks can be seen with varying Q. Both the temperature and wavevector dependence are in good agreement with the calculations of Glyde and Griffin. Their suggestion that the sharp single-excitation peak arises from the Bose condensate is supported by its disappearance above T_λ. We have demonstrated that the energy of the sharp peak never exceeds the two-roton energy 2Δ at any wavevector at this pressure.

Acknowledgments

We acknowledge the financial support of the UK Engineering and Physical Sciences Research Council. We have benefited from stimulating discussions with Mark Adams. We would like to thank the technical staff of ISIS; we are particularly grateful to Richard Down for his assistance on the beamline.

References

[1] Glyde H R, Gibbs M R, Stirling W G and Adams M A 1998 *Europhys. Lett.* **43** 422
[2] Glyde H R and Griffin A 1990 *Phys. Rev. Lett.* **65** 1454
[3] Glyde H R 1992 *Phys. Rev.* B 7321
[4] Fåk B and Andersen K H 1991 *Phys. Lett.* A **160** 469
[5] Fåk B, Regnault L P and Bossy J 1992 *J. Low Temp. Phys.* **89** 345
[6] Fåk B and Bossy J 1998 *J. Low Temp. Phys.* **112** 1
[7] Fåk B and Bossy J 1998 *J. Low Temp. Phys.* **113** 531
[8] Pitaevskii L P 1959 *Sov. Phys.–JETP* **9** 830

[9] Cowley R A and Woods A D B 1971 *Can. J. Phys.* **49** 177
[10] Smith A J, Cowley R A, Woods A D B, Stirling W G and Martel P 1977 *J. Phys. C: Solid State Phys.* **10** 543
[11] Adams M A 1997 *ISIS Technical Report* RAL-TR-1998-052
[12] Crevecoeur R M, DeGraaf L A, Montfrooij W, Svensson E C and Carlile C J 1995 *Nucl. Instrum. Methods Phys. Res.* A **356** 415
[13] Sears V F 1983 *Phys. Rev.* B **28** 5109
[14] Pearce J V, Azuah R T, Dimeo R M, Sokol P E, Stirling W G and Adams M A 2000 *Physica* B **276** 822
[15] Glyde H R, Azuah R T and Stirling W G 2000 *Phys. Rev.* B **62** 14 337